Lacunarity of the zero-crossings of Gaussian processes

A. Ogunshemi, K. I. Hopcraft, and S. P. Preston
School of Mathematical Sciences, Applied Mathematics Division,
University of Nottingham, Nottingham, NG7 2RD, United Kingdom

A lacunarity analysis of the zero-crossings derived from Gaussian stochastic processes with oscillatory autocorrelation functions is evaluated and reveals distinct multi-scaling signatures depending on the smoothness and degree of anti-correlation of the process. These bear qualitative similarities and quantitative distinctions from an oscillatory deterministic signal and a Poisson random process both possessing the same mean interval-size between crossings. At very small and large scales compared with the correlation length of the random processes, the lacunarity is similar to the Poisson but exhibits significant departures from Poisson behaviour if there is a zero-frequency component to the process's power-spectrum. A comparison of exact results with the gliding box technique that is frequently used to determine lacunarity demonstrates its inherent bias.

I. INTRODUCTION

An important role that random processes play in the natural sciences is to represent the behaviours caused by variables that influence a system about which information is incomplete, entirely absent, or cannot be measured accurately. There are many statistical descriptors of stochastic processes that quantify different manifestations of randomness and the Gaussian process has received most attention, not least because its two statistical descriptors, the mean and autocorrelation function, provide a complete description of its multivariate behaviours [1]. However, this simplicity does not carry to processes derived from a Gaussian process; in particular the properties associated with its zero-crossings [2] still defy such a complete characterisation. The periods or intervals between successive zero-crossings, denoted by T, are variously referred to as the residence or return time and has found application to nonequilibrium physical systems ([3], and references therein), the statistical properties of random polynomials [4], to phenomena initiated or terminated by crossing a threshold (see [5, 6] and references therein). Whilst the intervals are primarily affected by the properties of smoothness and by the different scale-sizes encapsulated within the autocorrelation function, there are additional patterns influenced by long correlations between the intervals that familiar correlation measures fail to capture or describe adequately. The concept of lacunarity was introduced originally [7] to augment the statistical descriptors of fractal behaviours. This article extends its utility and shows that the zero-crossing process can present both previously encountered and novel lacunarity signatures depending on the autocorrelation properties of the underlying Gaussian process. A particular focus is the effect on zero-crossings of oscillatory autocorrelation functions, which lead to considerably richer behaviour [8] and serve as a non-trivial model with which to explore the effects of weak through to strong correlation. Lacunarity provides an additional tool to examine these effects and, as will be shown, reveals novel scaling behaviours caused by the oscillations and the degree of anti-correlation present in the underlying Gaussian process.

II. THEORETICAL PRELIMINARIES

Lacunarity is defined as

$$\Lambda(r) = \left\langle n^2(r)\right\rangle / \left\langle n(r)\right\rangle^2 = 1 + \mathrm{var}\left(n(r)\right) / \left\langle n(r)\right\rangle^2, \quad (1)$$

where $\langle\cdot\rangle$ denotes the ensemble or realisation average, and lacunarity measures departures from translational invariance of the number $n(r)$ of events falling within a 'box' of size r. In the present context the events are zero-crossings of a stationary Gaussian process $x(t)$, which is assumed to have zero mean, unit variance σ^2 and normalized autocorrelation $\langle x(0)x(\tau)\rangle / \sigma^2 = \rho(\tau)$. Lacunarity characterises the heterogeneity of a process with scale-size, and is sensitive to the appearance of gaps punctuating the sequence of events. Since Λ involves the ratio of two moments it is sensitive to differences in scale-size that characterise these, and changes to the slope of Λ indicate the emergence of different scaling behaviours in the fluctuations of the number of crossings.

A related measure for the dispersion of events is the Fano factor

$$F(r) = \mathrm{var}(n(r)) / \left\langle n(r)\right\rangle, \quad (2)$$

which serves to gauge departures from Poisson behaviour, for which $F=1$. This was used in [8] to characterise the zero-crossings of a Gaussian process, albeit for a range of box sizes commensurate with the mean interval length.

When considering data derived from processes of two or more dimensions, the shape, orientation and structure of the box has been shown to be important for obtaining accurate estimates of Λ [10], but in the one-dimensional case considered in this article the lacunarity can be calculated exactly using the properties of Gaussian processes, some relevant results for which are as follows.

The mean rate of crossings for Gaussian processes is [9] $\bar{R} = \sqrt{-\rho''(0)}/\pi$, with a mean number of $\langle n(r)\rangle = \bar{R}r$ crossings occurring in a box of size r, giving a mean interval length of $\langle T\rangle = 1/\bar{R}$. The variance in $n(r)$ is [11]

$$\mathrm{var}\left(n(r)\right) = \bar{R}r + 2\bar{R}\int_0^r (r-\tau)\left(U(\tau) - \bar{R}\right)\mathrm{d}\tau, \quad (3)$$

where

$$U(\tau) = \bar{R}^{-1}\pi^{-2}\left(1-\rho^2(\tau)\right)^{-3/2}\left[\left|A^2 - B^2\right|^{1/2}\right.$$

$$+ B\arctan\left(B\left|A^2-B^2\right|^{-1/2}\right)\Big],$$
$$A=-\rho''(0)\left[1-\rho^2(\tau)\right]-\rho'^2(\tau),$$
$$B=\rho''(\tau)\left[1-\rho^2(\tau)\right]+\rho(\tau)\rho'^2(\tau),$$

whence the variance increases linearly with r for large r. The integral in (3) can be evaluated by quadrature once $\rho(\tau)$ is specified, and is here assumed to have the forms

$$\rho_{ij}(\tau;a)=g_i(\tau)\,f_j(\tau;a), \tag{4}$$

with

$$f_j(\tau;a)=\begin{cases}\cos(a\tau), & j=1,\\ \cos^2\left(a\tau/\sqrt{2}\right)=\frac{1}{2}\left(1+\cos(\sqrt{2}at)\right), & j=2,\end{cases} \tag{5}$$

where $a\geq 0$ and $g_i(\tau)$ is a function with expansion near the origin

$$g_i(\tau)=1-\frac{1}{2}\left(\frac{\tau}{\ell}\right)^2+\mathcal{O}\Big(|\tau|^3\Big),$$

with consequence that the mean interval length is $\langle T\rangle=\pi\ell$ if $a=0$. Expansions of $g_i(\tau)$ having even powers of τ alone describe processes smooth to all orders, with the effect that the intervals are anti-bunched, i.e. repelled, from each other. In contrast, a sub-fractal process is one for which the derivative of the process is a fractal, and these obtain from the presence of a term $\mathcal{O}\Big(|\tau|^3\Big)$ in the expansion for $g_i(\tau)$. In this case the intervals are bunched, i.e. clustered, leading to higher variance of $n(r)$. The subscript i indexes different models as follows, which have been selected for having properties that enable exploring different aspects of smoothness and scale:

$$g_1(\tau)=\exp\left(-\frac{\tau^2}{2\ell^2}\right),\ \text{Gaussian},$$
$$g_2(\tau)=\frac{3}{2}\exp\left(-\frac{|\tau|}{\sqrt{3}\ell}\right)-\frac{1}{2}\exp\left(-\frac{\sqrt{3}\,|\tau|}{\ell}\right),\ \text{Wong [12]},$$
$$g_3(\tau)=\frac{\sin\left(\sqrt{3}\tau/\ell\right)}{\sqrt{3}\tau/\ell},\ \text{sinc},$$
$$g_4(\tau)=\sin\left[\frac{\pi}{2}\exp\left(-\frac{2}{\pi}\frac{|\tau|}{\ell}\right)\right],\ \text{exponential}. \tag{6}$$

The scale-size ℓ is set to unity hereafter. Models 1 and 3 are both infinitely differentiable while models 2 and 4 are sub-fractal. Models 1, 2 and 4 are exponentially bounded, whereas the envelope of model 3 decreases as τ^{-1}. The oscillations due to the sinusoid are necessary for model 3 to possess a physically realizable energy density spectrum—their absence would render the total power infinite and thereby unphysical. This requirement holds for any autocorrelation function decaying slower than τ^{-1}. The intervals described by model 4 are approximately exponentially distributed, as shown in the Appendix, but they are slightly positively correlated and therefore not consistent with a Poisson process. The oscillatory terms $f_j(\tau;a)$ are selected to illustrate the distinct and novel manifestations that oscillations in the autocorrelation can produce. While both are oscillatory, the cosine model has both positive and negative regions of correlation, whereas the cosine-squared model has only non-negative correlation, and lacunarity detects these distinctions. Inclusion of these oscillatory terms modifies the expansion near the origin the same way up to terms in τ^2 for both models:

$$\rho_{ij}(\tau;a)=1-\frac{1+a^2}{2}\tau^2+\mathcal{O}\Big(|\tau|^3\Big),$$

with the consequence that the mean interval length is reduced to $\langle T\rangle=\pi/\sqrt{1+a^2}\to\pi/a$, for large values of a, which is consistent with $x(t)$ having the half-period of a deterministic sinusoid. Consequently with increasing a, $x(t)$ appears progressively more regular, resembling the deterministic function $x_d(t;a)=\cos\left(\sqrt{1+a^2}t\right)$ that has the same mean interval length, but with variance of the intervals that scale as $a^{-7/2}$ and a^{-1} for the cosine and cosine-squared models respectively (see Fig. 3), as can be calculated accurately using a Markov chain assumption [13] and verified by simulation results. Consequently elements of stochasticity in $x(t)$ persist and are distinct from the superficial similarity of the process to $x_d(t)$; lacunarity is sensitive to these differences in behaviours and characterises variations manifested by the processes.

III. SIMULATION METHODS

For processes with prescribed autocorrelation functions, lacunarity can also be evaluated from simulations [8, 14] using either contiguous discrete boxes or the 'gliding box' method [15] to compute lacunarity (1). Suppose that the resolution of the simulation is Δt, selected to be much less than the correlation length of the process, and a realisation is of total length $L=N\Delta t$, where $N\gg 1$. The contiguous box method counts the number of crossing events falling within contiguous boxes of length r that are selected so that $\Delta t\ll r\ll L$, the latter inequality required to ensure that the effective sample size is sufficiently large that the variance in (1) is computed accurately. The procedure is repeated with progressively larger box sizes to reveal the scaling of the lacunarity with r. The largest box size that can be used is therefore governed by the length the realisation. The gliding box method involves, for a box of size r, counting the number of crossings as the box is 'glided' in increments of Δt along the realisation. This has the apparent effect of using the data more efficiently by increasing the sample size, but in fact the counts in boxes that overlap are correlated which impacts accuracy of the computed variance and hence lacunarity. It is therefore instructive to compare the contiguous box and gliding box techniques with the exact analytical results in order to evaluate their accuracy in terms of the volume of data available to compute the lacunarity. The gliding box technique has been employed extensively (e.g. [16] and references therein,

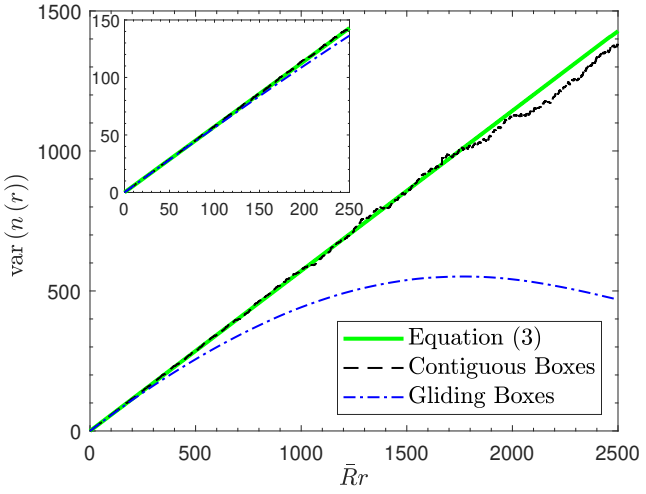

FIG. 1. A comparison between the exact and simulation estimates of var $(n(r))$ as a function of normalized box-size for the g_1 correlation function.

where further details for implementing the technique can be found) to measure lacunarity of small data sets where the precise nature of the stochastic process and its autocorrelation are unknown.

One way to simulate approximately a Gaussian process is the Fourier transform method, described for example in [8, 14], but iterative refinements to the generation method [17] ensure better accuracy, and for a Gaussian process this is verified by checking that the realisations conform to the higher-order properties they must satisty [18], viz. $\left\langle x^3(0)\,x(\tau)\right\rangle/\sigma^4 = 3\rho(\tau)$ and $\left\langle x^2(0)\,x^2(\tau)\right\rangle/\sigma^4 = 1+2\rho^2(\tau)$. Employing the contiguous box or gliding box techniques require care to ensure that box sizes are both significantly larger than the resolution of the simulation and significantly less than the total simulation length. Figure 1 illustrates the regime where estimates of Λ from data are accurate by displaying var $(n(r))$ as a function of normalized box size for the model g_1. The exact analytical result determined from equation (3) is displayed together with two empirical techniques based on 2000 computer-generated realisations with each simulation of length $\approx 5000\bar{R}^{-1}$. The result of the contiguous-boxes method agrees approximately with the exact results for $\bar{R}r \leq 1000$, corresponding to 5 or more contiguous boxes spanning each simulation's length. Although conspicuously less noisy, the gliding-box technique is nevertheless systematically biased and consistently underestimates both the magnitude and dependence of the variance on box size. The inset shows the region where both empirical methods accord with the exact result. Whilst simulations provide a wealth of information additional to that contained in moment-based measures, it is sufficient to use analytical results hereafter and to determine Λ using equation (3) and numerical quadrature.

IV. EXACT RESULTS

Figure 2 shows $\Lambda(r)$ as a function of normalized box-size $\bar{R}r$ for processes with autocorrelation functions $g_i(\tau)$, together with that for a Poisson process that is marginal between sub-fractal and smooth processes. The inset displays the dimensionless gradient $\gamma = \mathrm{d}\log(\Lambda-1)/\mathrm{d}\log(r)$ of these curves. For $\bar{R}r \ll 1$, $\Lambda = 1/\mathrm{Prob}\,(n(r)=1) \approx 1/\bar{R}r$, and so Λ is the same for all the processes, with $\gamma \approx -1$; indeed, this relationship is exact for the Poisson process which maintains a constant slope of -1 at *all* scales, a characteristic with which other processes may be compared for gauging the effect of correlation. For $10^{-1} < \bar{R}r < 1$, the smooth processes have fewer than two crossings in a box with high probability and so the fluctuations in number are essentially binomially distributed [14], with Λ less than the corresponding Poisson value and $\gamma < -1$. At larger r the Poisson and binomial fluctuations become asymptotically similar and the slope returns to -1, although the value of Λ remains less than that for the Poisson process. By contrast the fluctuations for the sub fractal processes are slightly greater than the Poisson case in the regime $10^{-1} < \bar{R}r < 1$ because clustering enables more than two crossings to occur within a box with higher probability than the smooth case, consistent with their number being negative-binomially distributed [14]. Consequently γ exceeds -1 but again the fluctuations scale asymptotically with the Poisson at larger r, now with Λ exceeding the Poisson value. Note that γ for the sinc-process has separate regimes where it is less than and greater than -1. Indeed, the derivative is oscillatory near $\bar{R}r = 1$, which is an artifact of the autocorrelation function being non-monotonic in this region. The envelope of this process is power-law, which is synonymous with intermittent 'bursts' of crossings, although these clusters are too infrequent and limited in scale to make the fluctuations super-Poisson. We shall now see how oscillations in the autocorrelation functions modify these results.

The energy density spectra associated with the autocorrelation functions reveal how the oscillatory terms localise power in the limit of large values of a and whether the oscillations affect the processes when compared with those described by the $g_i(\tau)$ functions alone. The energy density spectrum is

$$E(\omega) = \frac{1}{2\pi}\int_{-\infty}^{\infty} \rho(\tau)\cos(\omega\tau)\,\mathrm{d}\tau.$$

The key difference between the two oscillatory classes of autocorrelation function is that the cosine-squared models possess significant energy at zero-frequency by virtue of having always non-negative correlation. The effect is that energy is directed to the non-oscillatory part of the spectrum, as described by the $g_i(\tau)$. In contrast, the cosine models are positively and negatively correlated with the effect that the energy becomes concentrated in a narrow interval about the frequency of oscillation, a. This explains the differences in the variances of the interval

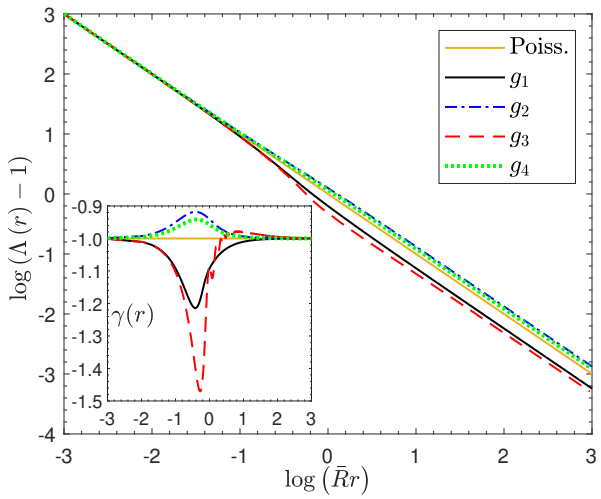

FIG. 2. Lacunarity and its dimensionless slope (inset) for processes with autocorrelation functions g_i together with the Poisson case for reference.

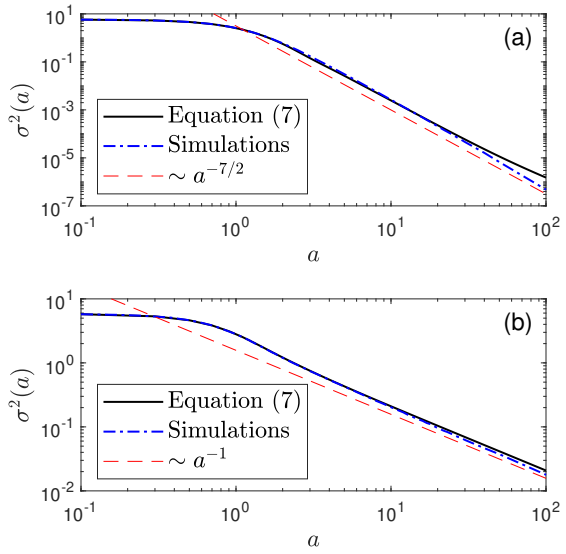

FIG. 3. Plots of the interval variance as the periodicity parameter a increases for processes with autocorrelation functions (a) $g_1(\tau)\cos(a\tau)$ and (b) $g_1(\tau)\cos^2\left(a\tau/\sqrt{2}\right)$. Dashed red lines indicate reference scalings of the simulation variance at large a.

lengths. Figure 3 illustrates the asymptotic forms of the variance of zero-crossing intervals for the two oscillatory modifications of the square exponential process, g_1. The plots include the analytic variance predicted by McFadden's work [13] for intervals from a Gaussian process,

$$\begin{aligned}\sigma^2 &= \sigma_1\sigma_2,\\ \sigma_1^2 &= 4\pi^{-1}\bar{R}^{-1}\int_0^\infty \arcsin\left(\rho(\tau)\right)\mathrm{d}\tau,\\ \sigma_2^2 &= \bar{R}^{-2}\left[1+2\int_0^\infty \left(U(\tau)-\bar{R}\right)\mathrm{d}\tau\right],\end{aligned} \qquad (7)$$

where $\rho(\tau)$ is the process's autocorrelation and $U(\tau)$ is the same function as in (3), and simulation estimates of the interval variance obtained as averages over 100 realisations for each value of $a \in \left[10^{-1}, 10^2\right]$. For the broadband cosine-squared processes the variances scale (approximately) as a^{-1} whereas for the narrowband cosine processes the scaling is the more rapid $a^{-7/2}$.

Figure 4(a) shows $\Lambda(r)$ for the processes with autocorrelation $g_i(\tau)\cos(a\tau)$ with $a=10$ together with the curve for $x_d(t)$ which is periodic. These periodicities are displayed in the inset and occur because within any normalized box length, $\mathrm{var}(n(r))$ is the product of the probabilities of a single crossing either appearing or not. The main figure displays the peak-to-peak value of Λ for $\bar{R}r > 7/2$ (the third maximum point after $\bar{R}r=1$), which decreases as $\left(\bar{R}r\right)^{-2}$, and so $\gamma=-2$. The periodicities are evident for the processes too, but the fluctuations are small rather than vanish when the box-size coincides with multiples of the mean interval length and the inset shows the oscillations decohere. The curves are similar to the Poisson with $\gamma\to-1$ for $\bar{R}r\geq 10$. Figure 4(b) shows Λ for the $g_i(\tau)\cos^2(a\tau)$ autocorrelation functions with the Poisson case shown for comparison. The periodicities are now vestigial and the Λ have a greater resemblance to the lacunarity for the g_i's because the power spectrum has a zero-frequency component that does not overlap substantially with the contribution due to the oscillations of ρ. However there is a distinct change in the slope for all the processes at $\bar{R}r=\sqrt{2}$ before γ eventually saturates at the Poisson asymptote when $\bar{R}r \gg 1$.

Figure 5(a–d) shows Λ and γ curves that result when $a=100$. Figure 5(a) is qualitatively similar to Fig. 4(a) because most of the power is concentrated about $\omega \sim a$, with little power in the zero-frequency part of the spectrum where differences between the sub-fractal and smooth processes are most evident; the inset highlights the oscillatory behaviour. The γ's for these processes are shown in Fig. 5(c) and detects the periodicities; for $\bar{R}r > 7/2$ the peak-to-peak slopes are shown, and these are qualitatively different to those presented in Fig. 2, becoming similar with the Poisson asymptote only for $\bar{R}r > 1000$. Figure 5(b) is for the $g_i(\tau)\cos^2(a\tau)$ autocorrelation functions and shows a region $1\leq\bar{R}r/\sqrt{2}\leq 10$ where Λ does not change significantly, indicative of the crossings being correlated over the scale-size associated with the g_i. Although this region exhibits periodicities, as seen from the inset, these are weaker and have a more complex structure than those of Fig. 5(a) as shown by the corresponding curves for γ given in Fig. 5(d). Both Λ and γ are essentially indistinguishable for the smooth cases, but the sub-fractal case is quite different from these at $\bar{R}r \gg 1$, and for all cases the value of Λ is some 1 or 3 orders of magnitude greater than those for the non-oscillatory and oscillatory autocorrelation functions respectively. Another distinguishing feature between plots

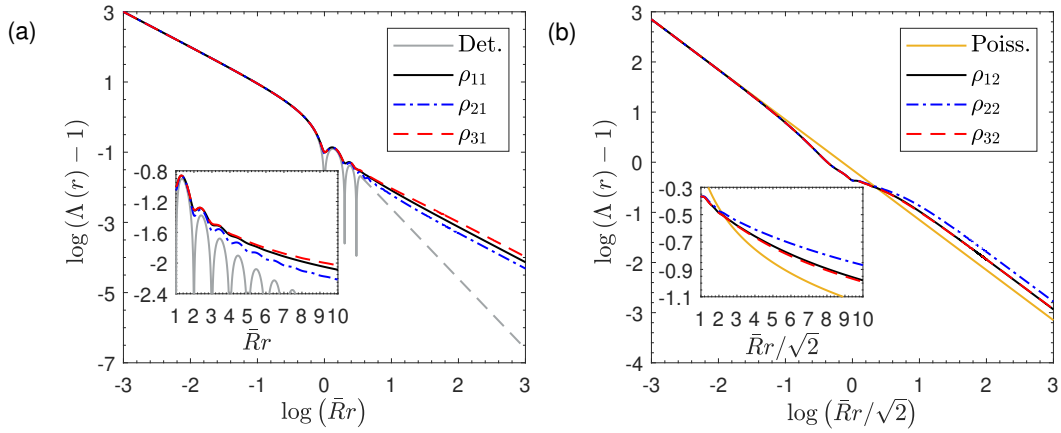

FIG. 4. Lacunarity curves for processes with oscillatory autocorrelation functions (a) $g_i(\tau)\cos(a\tau)$ and the deterministic signal with the same period, and (b) $g_i(\tau)\cos^2\left(a\tau/\sqrt{2}\right)$ with the non-oscillatory Poisson curve, when $a=10$. Insets show the periodicities that occur when box-sizes match multiples of the mean interval length. Within the main plot in (a), for $\bar{R}r\geq 7/2$ the peak-to-peak lacunarity values for the deterministic signal are plotted as a dashed grey line. The inset in (a) shows that peaks of the full lacunaity curve occur when r is an odd multiple of $\bar{R}^{-1}$.

(c) and (d) in Fig. 5 is that γ declines rather than rises towards the Poisson asymptote.

Figure 6(a) shows an extended sequence of normalized interval lengths obtained from a realisation with ρ_{11} when $a=100$, with a shorter range of the sample function included in Fig. 6(b). The intervals exhibit few excursions beyond 1.5 standard deviations from the mean, shown by the horizontal lines. This is because $\mathrm{var}(T)/\langle T\rangle \sim a^{-5/2}\ll 1$ and the correlation coefficient between successive intervals T and T', $\kappa=\left(\langle TT'\rangle-\langle T\rangle^2\right)/\mathrm{var}(T)\approx 0.65$, so the sequence of intervals forms an auto-regressive process with brief extremal excursions away from the mean. A realisation resembles a sinusoid of frequency $a/(2\pi)$ with slowly varying amplitude and phase occurring on the scale-size characterising $g_i(\tau)$ that slightly modulates the mean interval length. Contrast this with Fig. 6(c) obtained from a realisation with the autocorrelation function ρ_{12} , for which $\mathrm{var}(T)/\langle T\rangle\sim 1$. Now the excursions are of persistent significant size, and κ is negative since long intervals tend to be followed by shorter ones. The sequence of intervals therefore flips sequentially between the two branches that are symmetrically arranged about the normalized mode. A realisation resembles a slowly changing random process described by $g_i(\tau)$ upon which is superimposed a rapid sinusoidal modulation of frequency $a/(\sqrt{2}\pi)$. There are epochs when the amplitude and phases of these two primary components are such that no axis crossings occur as displayed in Fig. 6(d), leading to the lacunae that enhanced values of Λ measure.

V. SUMMARY AND DISCUSSION

The lacunarity of the zero-crossings of correlated Gaussian random processes display multiple-scaling signatures with box-size whose character depends on the smoothness and degree of anti-correlation of the process. Sub-fractal and smooth processes have Λ values that are respectively greater and less than a Poisson process, but are asymptotic to the Poisson value for box sizes much less than and much greater than the scale-size that characterizes the correlation properties of the underlying process.

Processes with oscillatory autocorrelation functions fall into two distinct classes depending on whether there is significant anti correlation. This property is equivalent to the energy spectrum $E(\omega)$ having two properties, the first being that $E(\omega)$ is concentrated about the oscillation frequency a and the second is that $E(0)$ is small compared with $E(a)$. These processes will exhibit periodicities in Λ similar to a deterministic sinusoid of the same interval length, but with peak-to-peak value of $\gamma\to -1$ rather than -2, which is the value a deterministic signal adopts.

Oscillatory autocorrelation functions that are nevertheless positively correlated always have a significant value of $E(0)$ that may be comparable or exceed the value of $E(a)$. Whilst the lacunarity for these processes exhibits vestigial periodicities for $\bar{R}r\sim 1$, the energy in the non-oscillatory part of the spectrum is dominant, leading to an intermediate plateau scaling regime where the lacunarity is approximately constant. This is a manifestation of the behaviour featuring in Figure 6(d), where the envelope of the process, whose scale-size is characterised by $g_i(\tau)$, does not cross the axis. This leads to a very long interval punctuating the regular short-intervals. These short-intervals resume once the envelope re-crosses

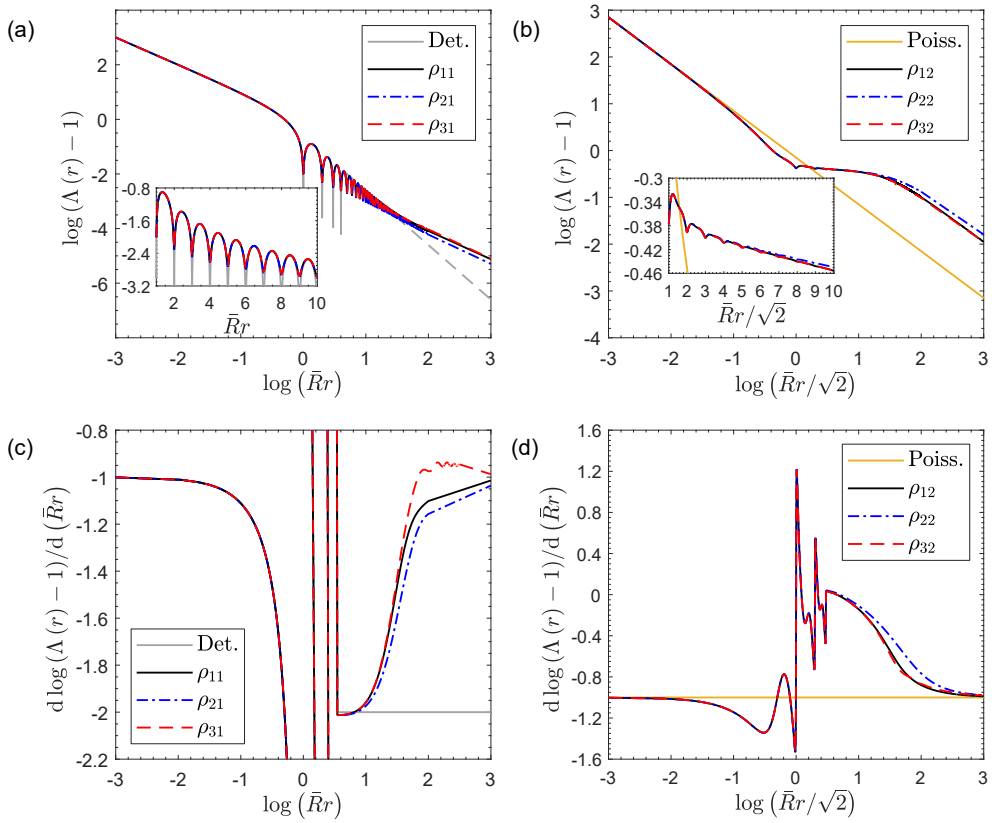

FIG. 5. Lacunarity and dimensionless slope curves for processes with oscillatory autocorrelation functions $g_i(\tau)\cos(a\tau)$ (a & c), and $g_i(\tau)\cos^2\left(a\tau/\sqrt{2}\right)$ (b & d), when $a=100$, compared with the deterministic signal with the same period and the non-oscillatory Poisson process. Within the main plot in (a), for $\bar{R}r>7/2$ the peak-to-peak lacunarity values for the deterministic signal are plotted as a dashed grey line, and in (c) the corresponding lacunarity slope as a solid grey line. The inset in (a) shows that peaks of the full lacunaity curve occur when r is an odd multiple of $\bar{R}^{-1}$.

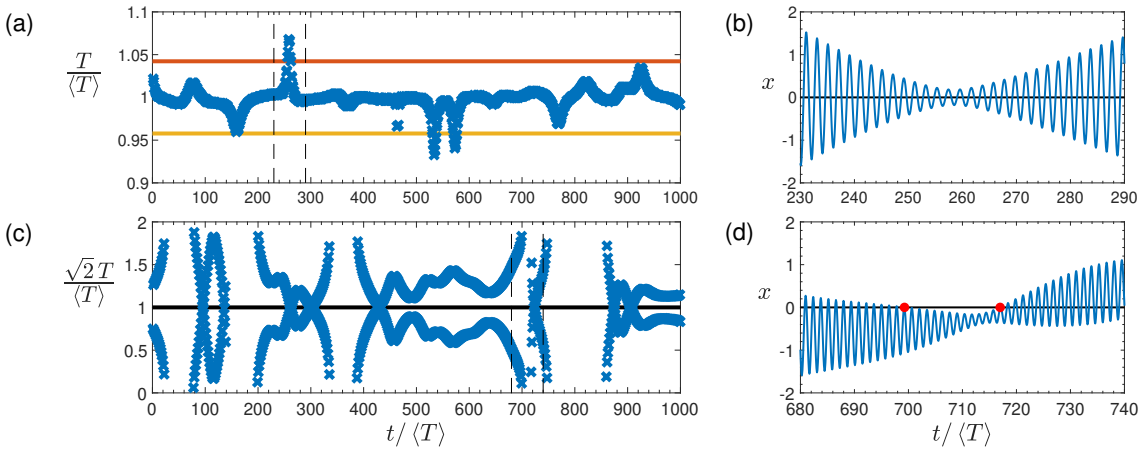

FIG. 6. Sequences (a & c) illustrating the correlation of zero-crossing intervals, and sample functions (b & d) showing the different types of periodicity, when $a=100$. Plots (a) and (b) are for the process ρ_{11}, and horizontal lines in (a) denote 1.5 standard deviations above (orange) and below (yellow) the mean. Plots (c) and (d) are for the process ρ_{12}, and the crossings flip between the two branches that are symmetrically disposed about the interval mode (horizontal black line), excursions greater than $\sqrt{2}\langle T\rangle$ occurring off-axis. Vertical dashed lines in plots (a) and (c) indicate the sections of the corresponding sample functions shown in (b) and (d), and the two red circles in (d) represent an interval of size $\approx 25\langle T\rangle/\sqrt{2}$.

the axis. Another manifestation of this behaviour is the quantitative differences between the processes formed by the sequence of zero-crossings that are derived from underlying processes that are positively correlated or have regions of anti correlation, as shown by Figure 6(a & c).

In accord with the case with non-oscillatory autocorrelation functions, the lacunarity slope eventually saturates with $\gamma \to -1$ at large normalized box sizes, although the values of $\bar{R}r$ at which this occurs are much larger. This shows the significant effect that oscillations in the autocorrelation function imbue.

VI. ACKNOWLEDGEMENTS

A.O. was supported by a PhD studentship funded by the University of Nottingham.

VII. APPENDIX

This appendix contains the derivation of the autocorrelation function, $g_4(\tau)$ defined in (6), for a Gaussian process with approximately exponentially distributed zero-crossing intervals.

The probability density function for intervals, T, distributed exponentially with mean $\langle T \rangle$ is

$$P(t) = \frac{1}{\langle T \rangle} \exp\left(-\frac{t}{\langle T \rangle}\right).$$

This has Laplace transform

$$\mathcal{L}\left[P(t)\right] = p(s) = \frac{1}{1 + \langle T \rangle s} = \frac{h(s)}{1 - h(s)},$$

say, if the intervals are assumed to be approximately independent, where [13]

$$\begin{aligned} h(s) &= \frac{1}{2} + \frac{s\langle T \rangle}{2\pi} \int_0^\infty \exp(-s\tau) \frac{g_4'(\tau)}{\sqrt{1 - g_4(\tau)^2}} \mathrm{d}\tau, \\ &= \frac{1}{2} + \frac{s\langle T \rangle}{2\pi} \int_0^\infty \exp(-s\tau) \frac{\mathrm{d}}{\mathrm{d}\tau} \sin^{-1}(g_4(\tau)) \mathrm{d}\tau. \end{aligned}$$

For exponential intervals

$$h(s) = \frac{p(s)}{1 + p(s)} = \frac{1}{2 + \langle T \rangle s}.$$

Hence

$$\int_0^\infty \exp(-s\tau) \frac{\mathrm{d}}{\mathrm{d}\tau} \sin^{-1}\left(g_4(\tau)\right) \mathrm{d}\tau = \frac{-\pi}{2 + \langle T \rangle s},$$

and taking the inverse Laplace transform obtains

$$\frac{\mathrm{d}}{\mathrm{d}\tau} \sin^{-1}\left(g_4(\tau)\right) = -\frac{\pi}{\langle T \rangle} \exp\left(-\frac{2\tau}{\langle T \rangle}\right).$$

Integrating,

$$\begin{aligned} \int_0^\tau \frac{\mathrm{d}}{\mathrm{d}t} \sin^{-1}\left(g_4(t)\right) \mathrm{d}t &= -\frac{\pi}{\langle T \rangle} \int_0^\tau \exp\left(-\frac{2t}{\langle T \rangle}\right) \mathrm{d}t, \\ \sin^{-1}\left(g_4(\tau)\right) - \sin^{-1}(1) &= -\frac{\pi}{2}\left(1 - \exp\left(-\frac{2\tau}{\langle T \rangle}\right)\right), \end{aligned}$$

then rearranging for $g_4(\tau)$, prescribing that $\langle T \rangle = \pi$, and replacing τ with $|\tau| / \ell$ gives (6), as required.

Note that $g_4(\tau)$ has a term $\mathcal{O}(|\tau^3|)$, so corresponds to a sub-fractal process. It can be approximated with good accuracy as

$$\frac{\pi}{2} \exp\left(-\frac{2\tau}{\pi}\right) - \left(\frac{\pi}{2} - 1\right) \exp\left(-\frac{\tau}{(\pi/2 - 1)}\right),$$

a form that can be used to evaluate an analytical approximation for the power spectrum of the process with oscillatory autocorrelation function $g_4(\tau)\cos(a\tau)$ as

$$E(\omega) = \frac{\pi\left(4 + \pi^2\left(a^2 + \omega^2\right)\right)}{(a\omega)^4 + \left(4 + (a\omega)^2\right)^2 + a^2\left(8\pi^2 - 2\pi^4\omega^2\right)} - \frac{(\pi - 2)^2\left(4 + a^2(\pi - 2)^2 + (\pi - 2)^2\omega^2\right)}{\pi\left(a^4(\pi - 2)^4 + 2a^2(\pi - 2)^2\left(4 - \omega^2(\pi - 2)^2\right) + \left(4 - \omega^2(\pi - 2)^2\right)^2\right)}.$$

[1] W. Feller, *An Introduction to Probability Theory and its Applications, Vol 2, 2nd Edition* (Wiley, New York, 1971).

[2] I. F. Blake, W. C. Lindsey, IEEE Trans. Inform. Theory **IT-19**, 295–315 (1973).

[3] G. C. M. A. Ehrhardt, S. N. Majumdar, A. J. Bray, Phys. Rev. E **69**, 016106 (2004).

[4] G. Schehr, S. N. Majumdar, Phys. Rev. Lett. **99**, 060603 (2007).

[5] M. I. Bogachev, J. F. Eichner, A. Bunde, Phys. Rev. Lett. **99**, 240601 (2007); B. Derrida, V. Hakim, R. Zeitak, *ibid.* **77**, 2871 (1996); S. N. Majumdar, C. Sire, A. J. Bray, S. J. Cornell, *ibid.* **77**, 2867 (1996); S. N. Majumdar, A. J. Bray, *ibid.* **86**, 3700 (2001).

[6] G. Lindgren, *Stationary Stochastic Processes: Theory and Applications* (Chapman & Hall/CRC, Boca Raton, 2013).

[7] B. Mandelbrot, *The Fractal Geometry of Nature* (Free-

man, New York, 1983).
[8] L. R. M. Wilson, K. I. Hopcraft, Phys. Rev. E **96**, 062129 (2017).
[9] S. O. Rice, in *Selected papers on noise and stochastic processes*, edited by N. Wax (Dover, New York, 1958).
[10] E. P. Rodrigues, M. S. Barbosa, L. F. Costa, Phys. Rev. E **72**, 016707 (2005).
[11] H. Steinberg, P. M. Schultheiss, C. A. Wogrin, F. Zweig, J. Appl. Phys. **26**, 195 (1955); D. Middleton, *An Introduction to Statistical Communication Theory* (McGraw-Hill, New York, 1960).
[12] E. Wong, SIAM J. Appl. Math. **14**, 1246 (1961).
[13] J. A. McFadden, IRE Trans. Inf. Theory, **4**, 14–24 (1958).
[14] J. M. Smith, K. I. Hopcraft, E. Jakeman, Phys. Rev. E **77**, 031112 (2008).
[15] C. Allain, M. Cloitre, Phys. Rev. A **44**, 3552 (1991).
[16] R. E. Plotnick, R. H. Gardner, W. W. Hargrove, K. Prestegaard, M. Perlmutter, Phys. Rev. E **53**, 5461 (1996).
[17] J. F. Eichner, J. W. Kantelhardt, A. Bunde, S. Havlin, Phys. Rev. E **75**, 011128 (2007).
[18] J. W. Goodman, *Statistical Optics* (Wiley, New York, 1984).